

# Poisson-Spot Intensity Reduction with a Partially-Transparent Petal-Shaped Optical Mask

Shahram Shiri <sup>1,\*</sup>, Wasył Wasyłkiwskyj, <sup>2</sup>

<sup>1</sup>*Optics Branch, NASA/Goddard Space Flight Center, Greenbelt, MD 20771, USA*

<sup>2</sup>*Electrical and Computer Engineering Department, The George Washington University, Washington, D.C. 20037, USA*

*Corresponding author: [ron.shiri@nasa.gov](mailto:ron.shiri@nasa.gov)*

## Abstract

The presence of Poisson's spot, also known as the spot of Arago, formed along the optical axis in the geometrical shadow behind an obstruction, has been known since the 18<sup>th</sup> century. The presence of this spot can best be described as the consequence of constructive interference of light waves diffracted on the edge of the obstruction where its central position can be determined by the symmetry of the object. More recently, the elimination of this spot has received attention in the fields of particle physics, high-energy lasers, astronomy and lithography. In this paper, we introduce a novel, partially transparent petaled mask shape that suppresses the bright spot by up to 10 orders of magnitude in intensity, with powerful applications to many of the above fields. The optimization technique formulated in this design can identify mask shapes having partial transparency only near the petal tips.

## 1. Introduction

The phenomenon of Poisson's spot, a bright spot in the shadow of circular disk, plays an important historical role in debates about the wave vs. particle nature of light. In 1818, hoping to disprove the conjecture that light is a wave, Simeon Poisson submitted a paper in a scientific competition sponsored by the French Academy of Sciences wherein he

deduced the 'outrageous' conclusion that if light were a wave, there would be a bright spot in the center of a shadow cast by a round opaque object. Much to his irritation, one of the Academy judges, Dominique Arago, performed the experiment and observed the resulting bright spot at the center of the diffraction pattern. Subsequent interest in this phenomenon appeared to recede, primarily being mentioned only in its historical context. More recently, interest in the Poisson spot has been revived in high-energy laser systems, optical lithography, observations of beam halo, and astronomy. In certain annular high-energy laser systems, there are substantial flux levels deposited at inconvenient locations throughout the system; some attempts to solve this problem by simple shadowing techniques are inherently impossible due to the nature of the diffraction process that produces the bright spot [1]. In conventional optical lithography, the presence of the unwelcomed bright spot causes a distortion of the original mask pattern during exposure [2]. The observation of beam halo or tail at the Photon Factory synchrotron & storage ring in Tsukuba, Japan, using a simple opaque disk, has been successful to a limited degree. The main idea is to block the glare of central image and to observe a hidden image such as beam tail [3]. In the astronomy community, elimination of the diffraction due to a circular aperture, suppression of the bright starlight in attempts to image an exoplanet [4] and suppression of side-lobe response in the bolometer array camera functioning in millimeter and sub-millimeter space telescopes are a few of examples of the need to suppress the Poisson spot [5].

In recent years, many researchers have attempted to analyze and characterize the Poisson spot [6] and determine its properties in the presence of the elementary aberrations with potential values for the wavefront analysis [7]. Similarly, the astronomy community has

been more active in pursuit of eliminating the Poisson spot. These researchers, with limited success, have studied various intensity-reduction techniques using circular transparency (apodized) masks and symmetric binary petaled occulters to reduce the intensity along the optical axis in the shadow [8] [9] [10] [11]. The circular transparency masks can be designed to reduce the optical-axis intensity sufficiently, but for freestanding mask applications, manufacturing a soft-edge smooth circular mask to the required accuracy is a daunting task. Conversely, binary petaled masks used as external occulters can be manufactured accurately, but are limited in their ability to achieve the intensity reduction in the desired spectrum range. This limitation arises from the fact that the radius-of-curvature at the petal tips is correlated to the intensity reduction along the optical axis. This recent finding was developed mathematically [12] and a comparison of the suppression from different petal tips (squared or round) has been presented [13].

In this paper, we build on earlier analytical work on the totally opaque petal mask and the partially transparent circular mask [12], considering a physical-optics analysis of a petal-shaped boundary having partial transparency at the petal ends to suppress the intensity along the optical axis. This novel class of masks allows the radii of curvature at the petal ends to be increased to physically realizable values while maintaining significant levels of intensity reduction. Even though this formulation is quite general, we have adhered to the parameters of the near-field diffraction geometry where the Fresnel number,  $F = R^2 / (\lambda z)$ , is much greater than one as shown in Figure 1. In this notation,  $R$  is the radius of mask,  $\lambda$  is the wavelength of incident beam, and  $z$  is the distance between the mask and detector.

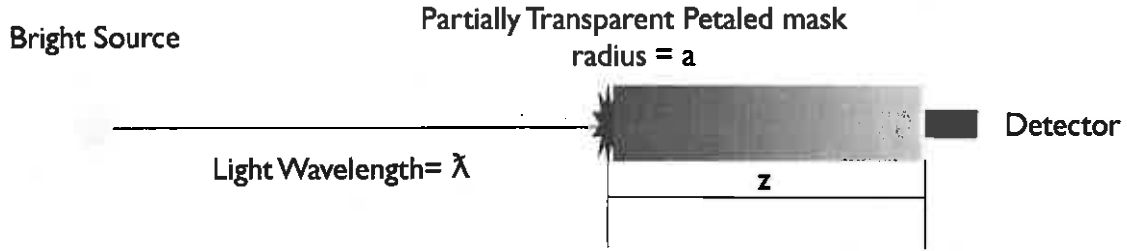


**Figure 1, Geometry of problem**

In Section 2, we summarize the mathematical formulation of Ref. [1] for the partially transparent petal-style mask. Here we express the electric field in the shadow zone of a mask with an arbitrary contour and explicitly identify the field along the optical axis. In Section 3, we review and compare the performance of the classic opaque petal-style mask and a partially transparent circular mask. In Section 4, we show that an optimally designed petal-style mask, employing a partial transparency near the petal tips, can extinguish the Poisson spot by more than 10 orders of magnitude. Such a mask would have significant advantages over the standard opaque petal mask (namely that the petal tips are substantially easier to fabricate, with tip radii of curvature on the order of centimeters rather than microns), and over the partially transparent circular mask (namely that the mask transparency extends only over a relatively small region near the petal tips rather than over the entire disk).

## 2. Analytical representation of the field in the mask shadow zone

From equation (A8) in Ref. [1], the field in the shadow zone of a mask is given by

$$E_y(\rho, z) = Ae^{-ik_0z} - A \int_0^{2\pi} d\varphi' \int_0^{R(\varphi')} [1 - T(\rho')] \rho' d\rho' \int_{-\infty}^{+\infty} \int_{-\infty}^{+\infty} e^{-k_i(\rho' - \rho)} d^2 \mathbf{k}_i \quad (1)$$

and the corresponding relative intensity by

$$I(\rho, z) = |E_y(\rho, z)|^2 / A^2 \quad (2)$$

The first term on the right of (1) is the field of an incident plane wave and the second term the scattered field [12];  $\rho$  is the radius in the observation coordinates  $(\rho, \varphi)$  normal to the  $z$ -axis,  $T(\rho')$  is the transparency function, which depends only on the distance from the coordinate center, and  $R(\varphi')$  is the functional form of the mask boundary. It can be shown [12] that, along the optical axis, the general expression (1) for the field can simplify to

$$E_y(0, z) = \frac{A}{2\pi} \int_0^{2\pi} d\varphi' \left\{ 1 - T[R(\varphi')] \right\} \frac{ze^{-ik_0\sqrt{z^2 + R(\varphi')^2}}}{\sqrt{z^2 + R(\varphi')^2}} + \frac{A}{2\pi} \int_0^{2\pi} d\varphi' \int_0^{R(\varphi')} d\rho' \frac{\partial T(\rho')}{\partial \rho'} \frac{ze^{-ik_0\sqrt{z^2 + \rho'^2}}}{\sqrt{z^2 + \rho'^2}} \quad (3)$$

In this form, the incident field together with the scattered field is merged into a single integral representation. Also, because the incident and scattered fields can differ by as little as  $10^{-10}$ , this representation has distinct computational advantages over Eq. (1), where the incident and scattered fields have to be subtracted directly. In addition, the contribution arising from the variation of the transparency function with the radial coordinate can be identified directly with the second term on the right containing the derivative. For a totally opaque structure, this term vanishes and, in addition,  $T(\rho') = 0$ . In this case, for a mask with a general contour  $R(\varphi')$  Eq. (3) reduces to

$$E_y(0, z) = \frac{A}{2\pi} \int_0^{2\pi} d\varphi' \frac{ze^{-ik_0\sqrt{z^2 + R(\varphi')^2}}}{\sqrt{z^2 + R(\varphi')^2}} \quad (4)$$

from which the field in the shadow on the optical axis of a petaled mask and of a constant-radius disk (yielding the Poisson spot intensity) follow as special cases. For points off the optical axis, a single representation incorporating the incident and scattered fields appears more difficult to construct. However a substantially simpler form, more amenable to computation than direct use of Eq. (1), is still possible. As shown in the Appendix, Eq. (1) can be transformed into

$$E_y(\rho, z) = A \left\{ e^{-ik_0 z} - \frac{ik_0}{2\pi z} e^{-ik_0 z} e^{-ik_0 \frac{\rho^2}{2z}} \int_0^{2\pi} d\varphi' \int_0^{R(\varphi')} [1 - T(\rho')] \rho' e^{-ik_0 \frac{\rho'^2}{2z}} e^{ik_0 \frac{\rho\rho' \cos(\varphi - \varphi')}{z}} d\rho' \right\} \quad (5)$$

involving a double integral instead of a quadruple integral. As a simplification, Eq. (5) uses the Fresnel approximation that is valid for the parameter range of interest herein. This approximation was not introduced earlier, in Eq. (3), because for this particular set of parameters, it would not have provided any computational advantages. One can show that, along the optical axis, Eq. (5) is identical with the Fresnel approximation of Eq. (3).

### 3. Comparison of opaque a petal-style mask and a partially transparent circular disk

In this section we employ the derivations from Ref. [12] and compare the intensity reductions achieved using a totally opaque petaled mask & a partially transparent circular mask (shown in Figure 2).



**Figure 2, Circular partially transparent mask and equivalent opaque petaled mask**

The radially tapered transparency mask considered here does not have petals and the functional form of the transparency has been chosen to minimize the average intensity over a prescribed interval of the optical axis; the designs of all masks analyzed in this present paper were made using the methodology outlined in Ref. [12]. The field in the mask shadow is evaluated using Eq. (4) for the totally opaque petal mask and a simplified version of Eq. (3) for the circular disk. Figure 3 shows a plot of the intensity along the optical axis as a function of the reciprocal of the Fresnel number for a mask with six petals designed for a visible range spectrum.

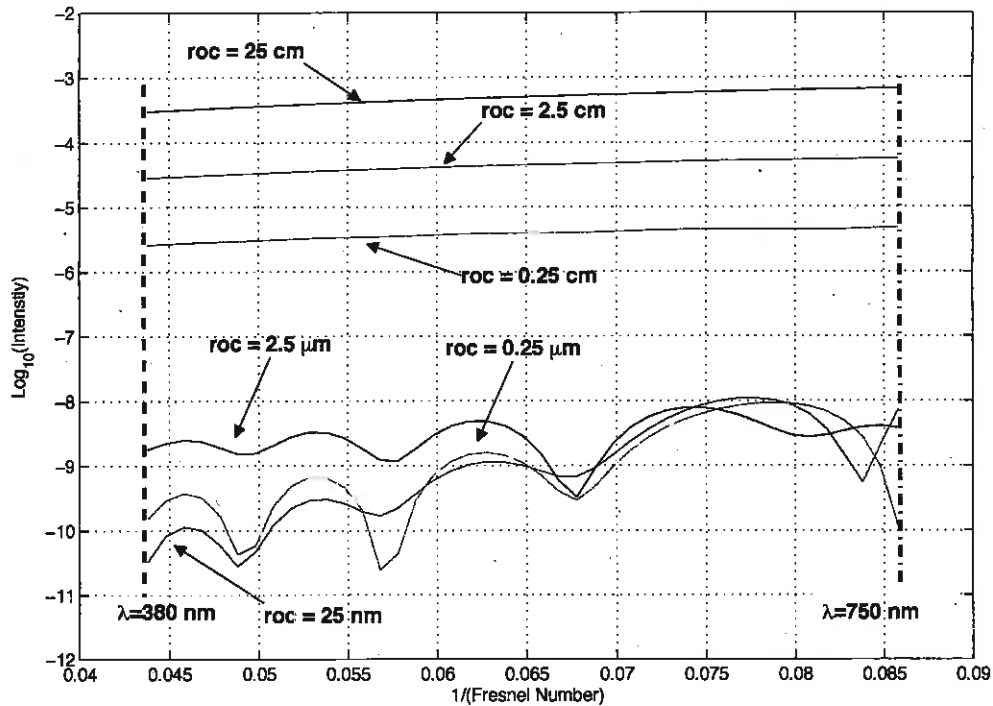


**Figure 3, Intensity reduction along optical axis when petal-style mask is used. The number of petals is preset to 6. As the radius of curvature (ROC) decreases, the intensity reduction increases.**

As the radius of curvature of the petal tips is progressively reduced from 25 cm to 25 nm, the intensity continues to decrease. We note that the results of Figure 3 predict that reaching a 10 order of magnitude reduction would require radii of curvature in the nanometer range; diffraction from such small structures by visible-wavelength light takes us outside the domain of the physical optics and so these results should not be taken literally. In the  $\sim$ micron and  $\sim$ mm range, where we can reasonably expect physical optics to hold, the intensity reduction is not too impressive.

Figure 4 shows a plot of the intensity along the optical axis as a function of the reciprocal of the Fresnel number for three partially transparent circular masks,

differing in the order of the polynomial in the transparency function using Eq. (A35) and (A37).

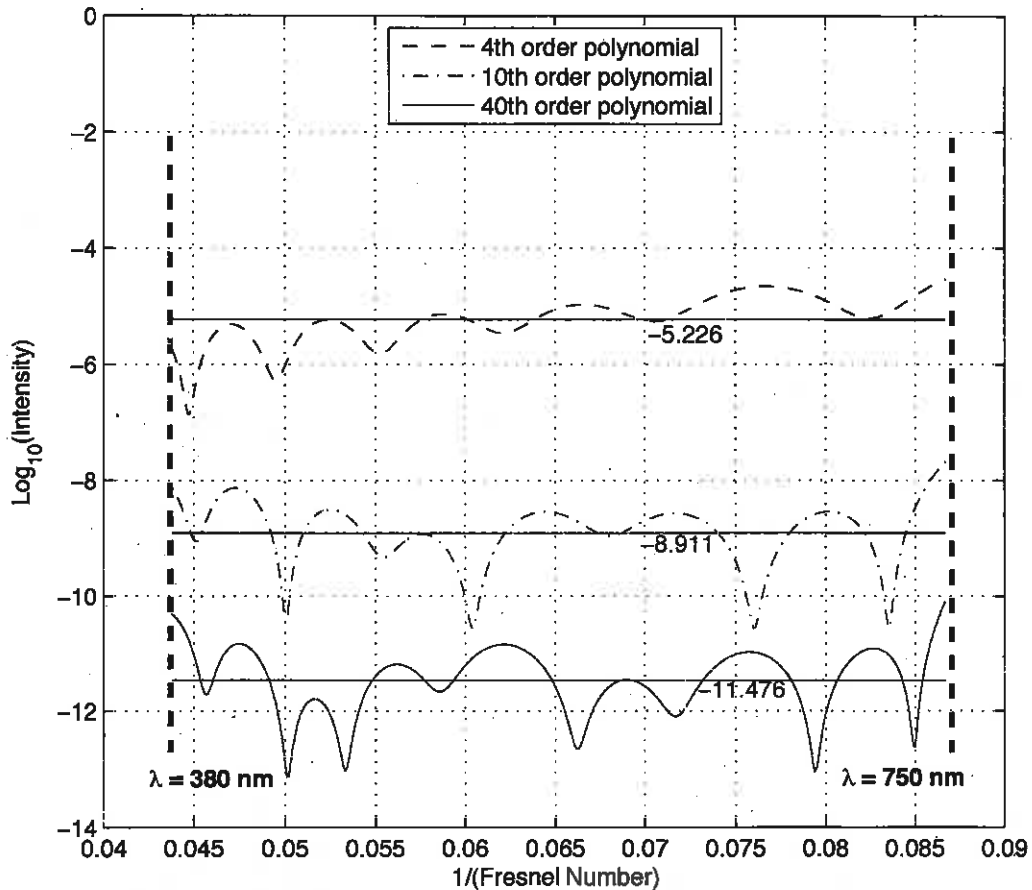


**Figure 4, Intensity on the optical axis of a circular partially transparent mask parameterized with the polynomial order of the transparency function.**

We note that as the order of the partial-transparency function polynomial is increased, the achievable intensity reduction also increases until the polynomial order reaches a maximum (in the present case 40) identified by the threshold in the associated singular value decomposition [12]. For this polynomial order the intensity reduction is comparable to that of the petal-style mask in Figure 3 provided the tip radii of curvature are reduced to the nanometer range.

#### 4. Petal-style masks with partially transparent petal ends

In order to overcome the requirement of physically unrealizable tip radii of curvature and a partial transparency that must cover the entire disk, we incorporate the petal style geometry together with a transparency into a class of hybrid masks, where the transparency is confined to a circularly symmetric region shown in Figure 5.

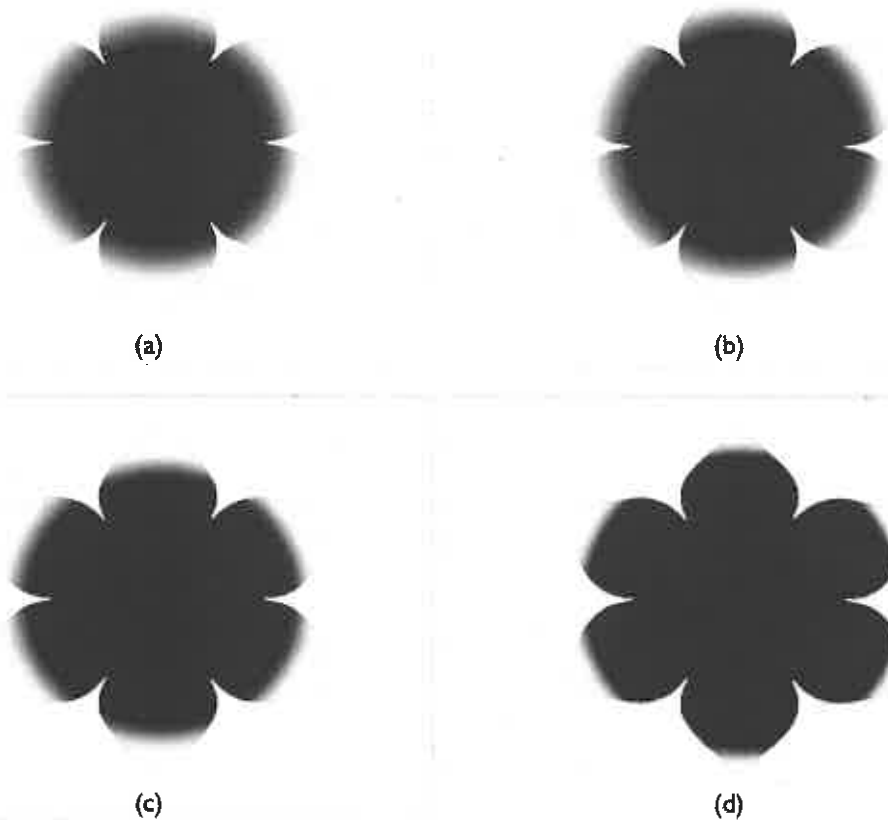


**Figure 5, Partially transparent 6-petal mask: (a) Offset at  $0.01R$  from the center of the disk. (b) Offset at  $0.25R$  from the center of disk. (c) Offset at  $0.5R$  from the center of disk. (d) Offset at  $0.75R$  from the center of disk. The edge of the petal is graphically highlighted for clarity.**

The key trade-off in this class of masks is that decreasing the radius of the opaque circular portion of the mask permits a proportional increase of the radii of curvature

at the petal tips. In the limit when the radius of the opaque inner circle in the mask approaches the outer mask radius, the tip radii curvature all-degenerate to the outer disk radius and the transparency covers the entire disk. In the "opposite" limit, as the diameter of the inner circle is allowed to approach 0, we obtain the classic petal style opaque mask with sharp petal tips.

Figure 5(a) represents the smallest opaque area at the center of the disk while Figs. 5(b)-(d) show opacity at  $0.25 \cdot R$ ,  $0.50 \cdot R$ , and  $0.75 \cdot R$  respectively of the normalized disk radius. The transparency-function profile associated with these masks, where the 'offset' shifts the beginning of the transparency, is depicted in Figure 6.

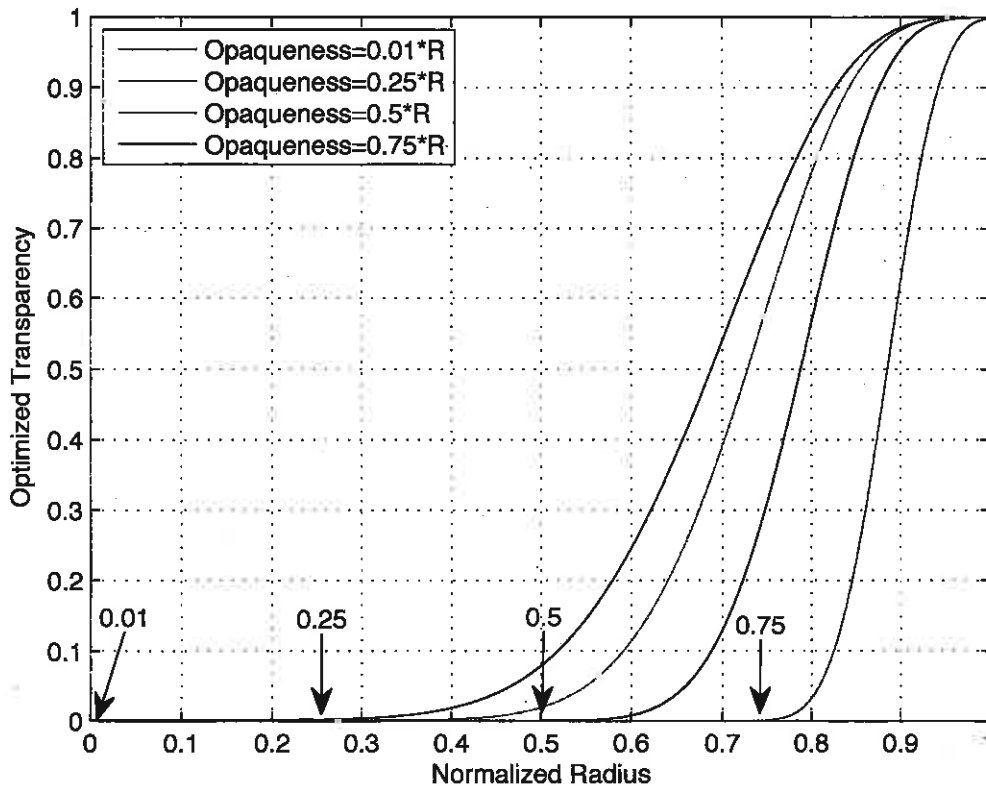
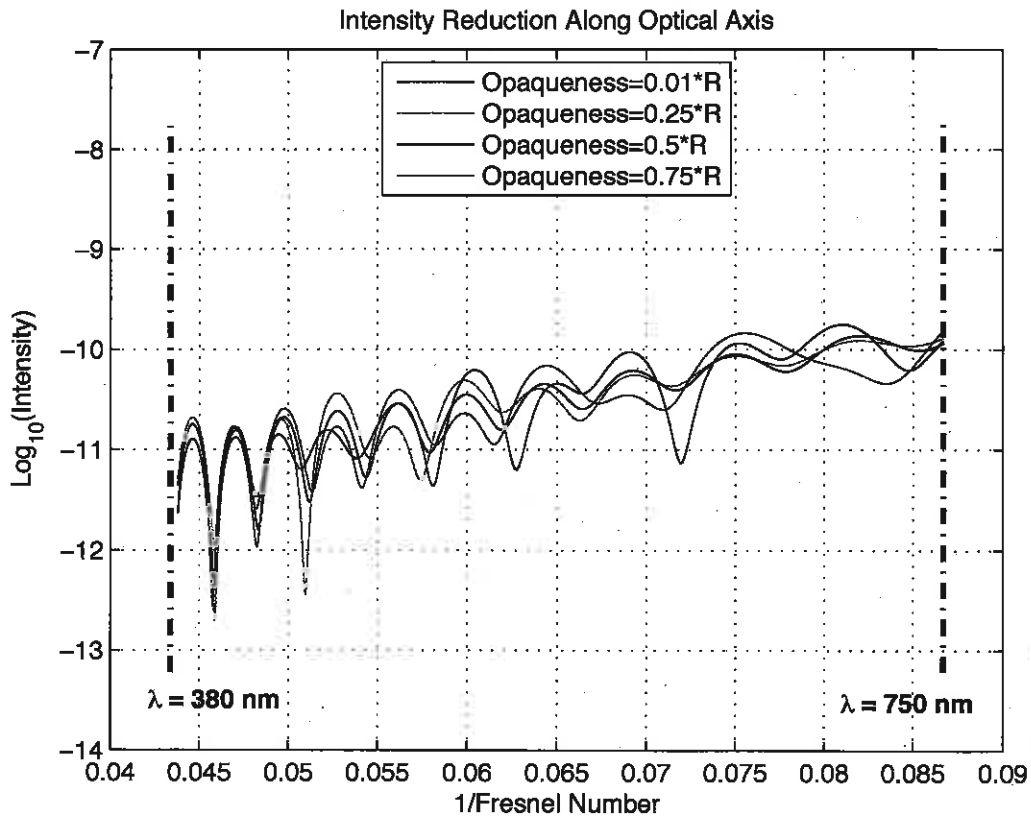


Figure 6, Transparent profile with 'offset' at 0.01, 0.25, 0.5, and 0.75 of the normalized radius.

The transparency profile, as shown in this figure, is not only shifted to larger normalized radii, but its general S-curve shape is altered due to the introduction of the 'offset' bias and optimization algorithm. Note that the slope of these transparency curves increases as the opacity is increased. The profile representing the smallest region of opacity ( $0.01 \cdot R$ ) is symbolically confined to a small region at the center to satisfy the assumption of this study where transparency is zero at the center of the disk. The profile with 'offset' set at  $0.75 \cdot R$  apparently has the sharpest slope. The radii of curvature of the 6-petal shape have been arbitrarily chosen to be 25 cm. The intensity reduction along the optical axis associated with these transparency profiles is shown in Figure 7.



**Figure 7, Intensity reduction along optical axis from partially transparent 6-petal shape mask.**

The location of 'offset' does not improve the intensity reduction substantially.

The changes in the opacity within the range of  $0.01 \cdot R$  to  $0.75 \cdot R$  do not improve the intensity reduction along the optical axis substantially. As a result, to better fabricate and manufacture such a mask, it is advantageous to obtain the optimized 'offset' position furthest away from the center of the disk. This observation implies an opacity covering a larger area of the disk, where only a small portion of the petal ends has a graduated transparency. Based on these results, the optimum transparency profile with the 6-petals occurs around  $0.785 \cdot R$ . The general shape of such a mask is shown in Figure 8.

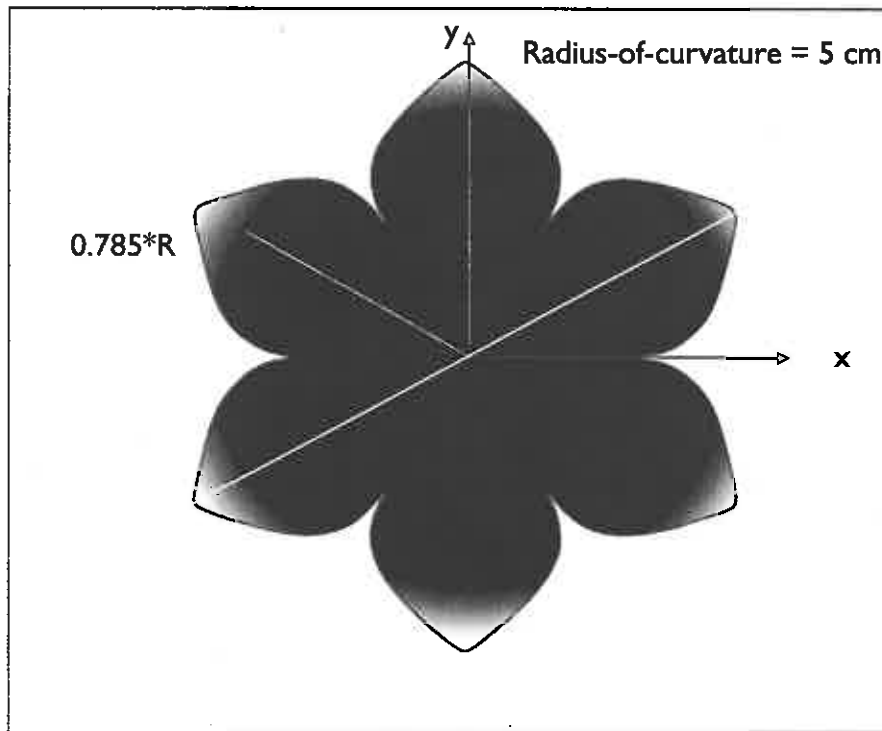


**Figure 8, Typical partially transparent 6-petal mask with 5-cm radius of curvature at the petal tips. The mask transparency is fully opaque for 78.5% of the mask. The edge of petal is graphically highlighted to mark the boundaries for the clarity.**

For the 6-petal mask with full opacity covering  $0.785 \cdot R$  of the radius, the petal tip radii could be adjusted from 50 microns to as large as 50 centimeter, and for each choice of tip radii, the partial transparency near the petal ends can be adjusted to

provide an optimized mask that significantly reduces the intensity along the optical axis. The area covered by the transparent portion of this mask is about 2% of the area of the circular disk. Compared with the fully transparent circular disk, this ratio represents significant reductions in the area that must be covered by a transparency and should substantially reduce the challenges to fabricate such masks.

It is important to note that the relative intensity does not depend explicitly on the radius of the disk or the distance between the disk and the observation point, but only on the reciprocal of the Fresnel Number at the observation point. In this study, we calculate the intensity numerically using Gaussian quadrature and employ high-resolution interpolation points between the fixed Legendre polynomial intervals with equal weighting functions. Figure 9 compares the intensity reduction due to three types of masks along the optical axis for light in the visible spectrum.

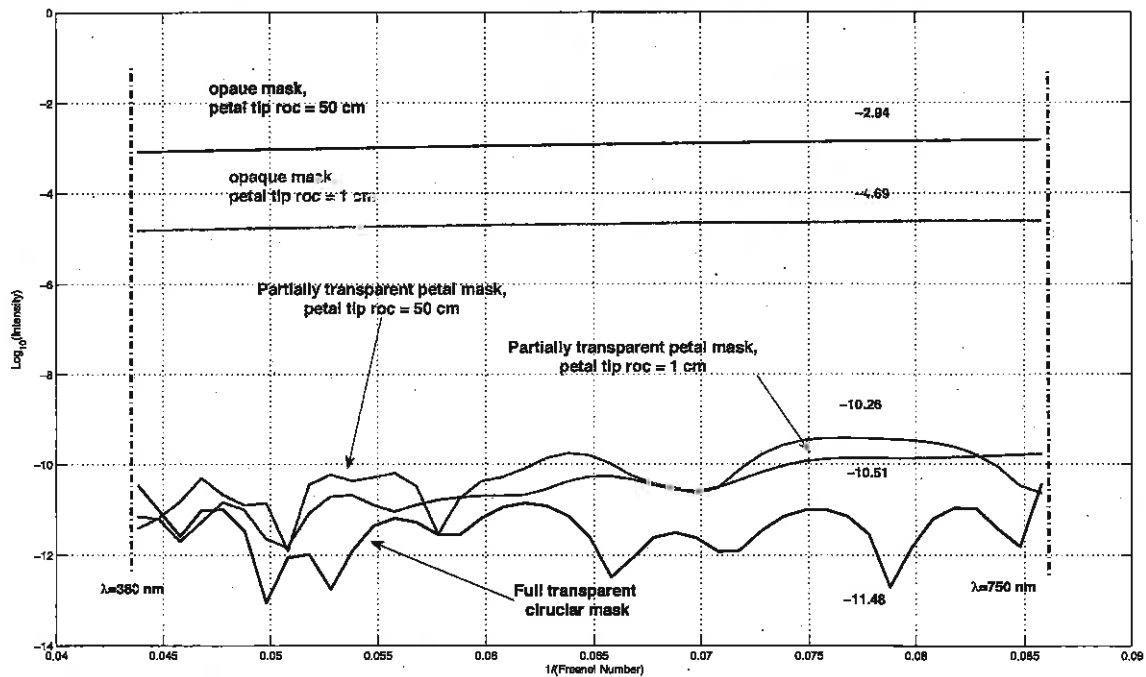


**Figure 9, Comparison of intensity reduction by three types of masks: the fully opaque petaled mask, the transparent circular mask and partially transparent petaled mask.**

The plots at the top of Figure 9 represent the intensity reduction obtained by opaque 6-petal masks with radii of curvature of 50 cm and 1 cm. The average intensity reduction in these cases is -2.94 and -4.69 orders of magnitude, respectively. The fully transparent circular mask, using a 40<sup>th</sup> order polynomial for the transparency function, shows the best performance. Closely following is the performance of the two partially transparent petaled masks. The optimized transparency in both cases has an 'offset' of  $0.785 \cdot R$ . The masks with 5 cm petal tip radii of curvature yields a mean log-intensity reduction of -10.26 and the mask with 1 cm tip radii of curvature has a reduction of -10.51. We should note the lack of sensitivity of this reduction to changes in the radii of curvature. By comparison, the same change in the radii of curvature in the totally opaque petal-style mask changes the intensity by about 2 orders of magnitude.

## **5. Conclusions**

It is desirable to effectively suppress the Poisson spot, present at the optical axis in the shadow of an object, in many disciplines, such as particle physics, high energy lasers, astronomy, and lithography. Our analysis of totally opaque petal-style masks and partially transparent circular masks show these masks can reduce the intensity along the optical axis and suppress the Poisson spot. However to obtain significant reduction, a partially transparent petaled style mask can reduce the intensity in the shadow zone along the optical axis by at least 10 orders of magnitude. A circular transparent disk with the same diameter of petaled mask could provide comparable

performance. It eliminates the difficulty of realizing small petal tip radii of curvature but introduces its own problem by requiring that the transparency cover the entire disk area. The approach proposed herein circumvents the difficulty associated with small petal tip radii of curvature as well as the transparency over the entire disk area. The novel partially transparent petaled mask employs a petal style boundary and a transparency that covers a relatively small area in the neighborhood of the petal end. As a consequence, the radii of curvature at the petal tips can be increased to substantially larger values than those in the totally opaque petal-style masks (e.g., centimeters as opposed to microns) and the area to which the transparency is applied can be reduced significantly, to about 2% of the mask area in the optimum design shown in Figure 8.

## Appendix

### An alternative representation of the field in the mask shadow

We start with the Fourier transform of the scalar Green's function

$$G(R) = \frac{1}{4\pi R} e^{-ik_0 R} = \frac{1}{(2\pi)^2} \int_{-\infty}^{\infty} \int_{-\infty}^{\infty} \frac{e^{-ik_i(\rho-\rho')} e^{-i\sqrt{k_0^2 - k_i^2} z}}{2i\sqrt{k_0^2 - k_i^2}} d^2 k_i \quad (A1)$$

where

$$R = \sqrt{|\boldsymbol{\rho} - \boldsymbol{\rho}'|^2 + z^2} \quad (A2)$$

Differentiating the rightmost expression of (A1) with respect to  $z$  we get

$$\frac{1}{(2\pi)^2} \int_{-\infty}^{+\infty} \int_{-\infty}^{+\infty} e^{-ik_t \cdot (\rho - \rho') - ik_z z} d^2 k_t = -2 \frac{\partial G}{\partial z} \quad (\text{A3})$$

On the other hand, differentiation of the first equality for G in Eq. (A1) yields

$$-2 \frac{\partial G}{\partial z} = \frac{1}{2\pi} \left\{ \frac{ik_0}{R} + \frac{1}{R^2} \right\} e^{-ik_0 R} \frac{z}{R} \quad (\text{A4})$$

A comparison of the scattered field represented by the second term on the right in (1) with the left side of (A3) shows that the scattered field can be written in the following form of polar coordinates:

$$E_y^s(\rho, z) = \frac{A}{2\pi} \int_0^{2\pi} d\varphi' \int_0^{R(\varphi')} [1 - T(\rho')] \rho' d\rho' \left( \frac{ik_0}{R} + \frac{1}{R^2} \right) \frac{z}{R} e^{-ik_0 R} \quad (\text{A5})$$

Within our parameter range,  $z/R \approx 1$  and  $k_0 R \gg 1$  so that

$$\frac{ik_0}{R} + \frac{1}{R^2} \approx \frac{ik_0}{R} \quad (\text{A6})$$

Introducing the Fresnel approximation, we have for the amplitude term  $R \approx z$  and for the phase

$$k_0 R = k_0 z \sqrt{1 + \frac{|\rho - \rho'|^2}{z^2}} \approx k_0 z + \frac{k_0}{2z} [\rho^2 + \rho'^2 - 2\rho\rho' \cos(\varphi - \varphi')] \quad (\text{A7})$$

With these approximations (A5) simplifies to

$$E_y^s(\rho, z) = \frac{A e^{-ik_0 z} e^{-ik_0 \frac{\rho^2}{2z}}}{2\pi z} \int_0^{2\pi} d\varphi' \int_0^{R(\varphi')} [1 - T(\rho')] \rho' d\rho' e^{-ik_0 \frac{\rho'^2}{2z}} e^{ik_0 \frac{\rho\rho' \cos(\varphi - \varphi')}{z}} \quad (\text{A8})$$

Subtracting this from the incident field we obtain (5).

## REFERENCES

- [1] A. E. Siegman, *Lasers*. Mill Valley, CA: University Science, pp. 862-864, 1986.
- [2] T. Shihing, X. Xiaoxiang, S. Wangning, L. Wuxia, L. Junjie, and G. Changzhi, "Large-scale ordered silicon microtube arrays fabricated by Poisson spot lithography," *Nanotechnology*, vol. 22, p. 395301, 2011.
- [3] T. Mitsuhashi, "Design and Construction of Coronagraph for Observation of Beam Halo," in *European Particle Accelerator Conference (EPAC'04)*, Lucerne, Switzerland, 2004, pp. 2655-2657.
- [4] R. G. Lyon, S. Heap, A. Lo, W. Cash, G. D. Starkman, R. J. Vanderbei, N. J. Kasdin, and C. J. Copi, "Externally occulted terrestrial planet finder coronagraph: Simulations and sensitivities - art. no. 668719," in *Uv/Optical/Ir Space Telescopes: Innovative Technologies and Concepts Iii*. vol. 6687, H. A. MacEwen and J. B. Breckinridge, Eds., ed, 2007, pp. 68719-68719.
- [5] S. Anders, T. May, V. Zakosarenko, K. Peiselt, E. Heinz, M. Starkloff, G. Zieger, E. Kreysa, G. Siringo, and H.-G. Meyer, "Cryogenic bolometers for astronomical observations in the sub-mm range," *Microelectronic Engineering*, vol. 88, pp. 2205-2207, 2011.
- [6] R. L. Lucke, "Rayleigh-Sommerfeld diffraction and Poisson's spot," *European Journal of Physics*, vol. 27, pp. 193-204, 2006.
- [7] J. E. Harvey and J. L. Forgham, "THE SPOT OF ARAGO - NEW RELEVANCE FOR AN OLD PHENOMENON," *American Journal of Physics*, vol. 52, pp. 243-247, 1984.
- [8] C. J. Copi, G. D. Starkman, L. Lichodziejewski, F. Kustas, W. Chun, and B. Easom, "The Big Occulting Steerable Satellite (BOSS)," *2000 IEEE Aerospace Conference Proceedings, Vol 7*, pp. 403-410 686, 2000.
- [9] P. Nisenson and C. Papaliolios, "Detection of earth-like planets using apodized telescopes," *Astrophysical Journal*, vol. 548, pp. L201-L205, Feb 2001.
- [10] W. Cash and A. Lo, "Tips for Starshade Design," *Journal of Optical Society of America A*, Under Review 2011.
- [11] R. J. Vanderbei, "Eliminating Poisson's Spot with Linear Programming," in *Operations Research and Cyber-Infrastructure*, J. W. Chinneck, B. Kristjansson, and M. J. Saltzman, Eds., ed, 2009, pp. 455-467.
- [12] W. Wasylkiwskyj and S. Shiri, "Limits on achievable intensity reduction with an optical occulter," *J. Opt. Soc. Am. A*, vol. 28, pp. 1668-1676, 2011.
- [13] W. Wasylkiwskyj and S. Shiri, "Response to 'Tips for Starshade Design'," *Journal of Optical Society of America A*, 2012.